EFFECT OF THE INTERNAL GAS FLOW VELOCITY ON THE THERMAL CONDUCTIVITY OF POROUS THERMAL PROTECTION SYSTEMS

Jérémy Chevalier[1,4]*, Bruno Dubroca*[3]*, Antonio Cosculluela*[4]*, Azita Ahmadi-Senichault*[2]*, Jean Lachaud*[1]

1 University of Bordeaux, Institute of Mechanical Engineering (I2M), 33400, Talence, France
2 Arts et Metiers Institute of Technology, Université de Bordeaux, CNRS, INRA, INP, I2M, HESAM Université, F-33400 Talence, France
3 University of Bordeaux, CNRS, CEA, Laboratoire des Composites Thermostructuraux (LCTS) 33600, Pessac, France.
4 CEA-CESTA, 15 avenue des Sablières, CS 60001, 33116 Le Barp Cedex 1, France.

ABSTRACT

Porous carbon fiber preforms, such as Calcarb and FiberForm, are used as reinforcements in Thermal Protection System (TPS) materials. Their effective conductivity is currently measured - or evaluated from tomographies - in static conditions. The thermal conductivity is therefore assumed to be a constant with respect to the flow velocity, ignoring dispersion effects induced by flows of pyrolysis or boundary layer gases within the structure. The objective of this study is to evaluate the relevance of this hypothesis, that is, estimate the influence of the flow velocity on the true thermal conductivity tensor of the material. The microscopic conservation equations for the gas phase (mass, momentum, energy) and the fibers (energy) are volume-averaged under the assumption of local thermal equilibrium and incompressible creeping flow. The effective conductivity can be expressed with three main terms: the first depends on the thermal conductivities and volume fractions of each phase, the second is a tortuosity term directly related to the microscopic structure of the object, and the third is a dispersion term related to the fluid velocity within the structure. It is the latter whose effect on thermal conductivity will be quantified here. A periodic closure model is implemented in the Porous material Analysis Toolbox based on OpenFOAM (PATO) to study the cases of arrays of solid cylinders. The results obtained are validated by comparison with the literature and extended to conditions relevant for the TPS application. The study is then applied to a 3D tomography of Carlcarb to determine at what flow velocity the dispersion is important by varying the Péclet number. The results are linked with experimental measurements, presented in a companion presentation (Experimental investigation of heat transfer in Calcarb : one or two temperature model ?, S. Liu et al.).

Index Terms— Effective thermal conductivity, Volume averaging, Péclet, Dispersion, Thermal Protection System, Calcarb, Micro-CT image, Pore-scale numerical simulations.

1. INTRODUCTION

During hypersonic atmospheric entry, space vehicles are submitted to intense heat fluxes [1, 2]. Thermal protection systems (TPS) are used to protect the payload. Porous materials are often selected as they combine light weight and reduced thermal conductivity. For example, porous ceramic materials were used to protect the Space Shuttle [3]. Porous ablative material have been actively developed during the last decades. A notable example is the Phenolic Impregnated Carbon Ablator (PICA) [4] that was employed for the heatshield of the Stardust capsule (2006) [5], the Mars Science Laboratory (2012) [6], Mars 2020 [7].
Numerical modeling of the response of a thermal protection material must be able to describe heat transfer with accuracy. Uncertainty propagation analyses have shown that the thermal conductivity is an essential parameter in TPS design [6, 8, 9]. The thermal conductivity is experimentally measured using techniques such as the Hot Disk (HD) or Laser Flash Analysis (LFA) [4]. These measurements are made in static conditions - i.e. no gas flow through the sample. The thermal conductivity is therefore assumed to be a constant with respect to the flow velocity. However, the thermal conductivity increases with the flow velocity. This effect is called dispersion [10]. Ignoring dispersion effects induced by flows of pyrolysis or boundary layer gases within the structure is a source of uncertainty for material response models. This hypothesis is acceptable as long as the Péclet number describing the ratio between convective and conductive effects remains small compared to 1, which is often considered true in the case of atmospheric entry. This parameter can change during the flight due to a high gas velocity or an increase in the characteristic pore length relative to cracks. In this context, it is important to quantify the impact of the convective effect in function of Péclet number. Experimental methods to quantify the convective impact are being developed, more details can be found in the article submitted by Shaolin Liu for the FAR conference 2022: " Experimental investigation of heat transfer in Calcarb : one or two temperature model?".

With the generalization of Computed X-Ray Tomography and parallel numerical simulations, numerical analyses are also carried out to improve our understanding of heat transfer in porous materials [11]. It remains a complex topic due to the coupling of conduction, convection and radiation. Panerai et al. studied the effective conductivity of carbon fiber preforms [12]. Nouri et al. studied conduction-radiation coupling [13]. In this work we will study conduction-convection coupling with the objective of evaluating the influence of the flow velocity on the true thermal conductivity tensor of the material. In the second section, the heat transfer equations are homogenized using the volume averaging method under the assumption of local thermal equilibrium between the fluid and solid regions [10, 14]. A closure problem is derived to allow computing the dispersion component of the effective conductivity from the intrinsic properties, microscopic architecture and flow velocity. In section three, this upscaling approach is applied to a periodic array of cylinders and validated by comparison with literature data. In section four, the strategy is applied to a tomography of Calcarb, which is the carbon preform of ASTERM, a porous carbon phenolic material developed by ArianeGroup for ESA missions.

2. VOLUME AVERAGING

Since the late 19th century, the multi-scale behavior of multiphase materials has been of research interest. The first works carried out made it possible to bring out the concept of effective properties. Nowadays, the determination of effective properties for multiphase media has applications in various types of materials and fields. Mention may be made of composite materials, biological and geological structures or building construction materials. Several methods have been developed [15]. In this work we will use the volume averaging theory. It will be presented and applied to our problem of interest.

2.1. Theory

Volume averaging relies on spatially averaging the microscopic partial differential equations to derive a set of macroscopic equations.

This method is used to derive continuity equations in a multiphase system like the one represented in Fig. 1. In other words, this means that the equations valid in each phase are spatially extended in order to obtain equations valid everywhere at the macroscopic scale. This methodology drastically simplifies the problem since it avoids the direct simulation at the scale of the pore by carrying out the modeling at the Darcy scale. As shown in the figure, two scales are considered. The first one is the microscopic scale encompassing the complex structure of the material with several phases, as seen in zoom of Fig. 1. The second one is the macroscopic scale where microstructural effects are taken into account in an average manner, which is generally sufficient for design purposes. Volume averaging produces satisfactory results if the condition Eq.(1) is satisfied [16, 15]

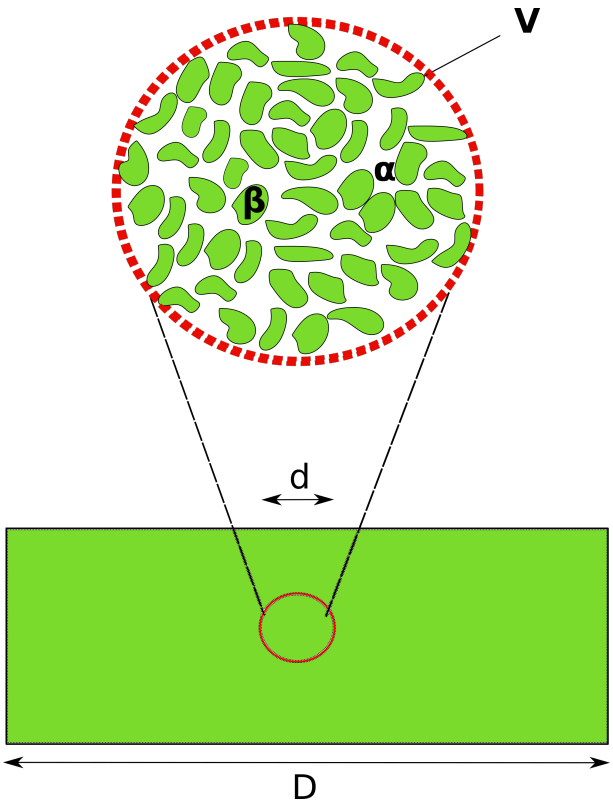

Fig. 1. Typical representative elementary volume (REV) for an arbitrary porous medium

$$l \ll d \ll D \tag{1}$$

where l is the characteristic length of the pores, d the characteristic length of the REV and D the characteristic length of the problem studied.
The definitions of the phase average and intrinsic phase average [17, 18] for a phase α are defined as

$$\begin{cases} \langle \cdot \rangle & = & \frac{1}{V} \int_{V_\alpha} \cdot \, \mathrm{d}V \\ \langle \cdot \rangle^\alpha & = & \frac{1}{V_\alpha} \int_{V_\alpha} \cdot \, \mathrm{d}V \end{cases} \tag{2}$$

and the associated operators are given by

$$\begin{cases} \langle \nabla \cdot \rangle & = & \nabla \langle \cdot \rangle + \frac{1}{V} \int_{A_{\alpha\beta}} \cdot \, \boldsymbol{n_{\alpha\beta}} \, \mathrm{d}A \\ \langle \frac{\partial \cdot}{\partial t} \rangle & = & \frac{\partial}{\partial t} \langle \cdot \rangle - \frac{1}{V} \int_{A_{\alpha\beta}} \cdot \, \boldsymbol{W} \cdot \boldsymbol{n_{\alpha\beta}} \, \mathrm{d}A \end{cases} \tag{3}$$

where V represents the representative elementary volume and V_α the volume occupied by the α-phase in V. $A_{\alpha\beta}$ is the area of the interface between the α and β phases, $\boldsymbol{W}$ is the

displacement vector of the interface and $\boldsymbol{n_{\alpha\beta}}$ the outgoing unit normal vector at the interface pointing from α-phase to β-phase.

A general microscopic mass transport equation of a property Ψ [17] is written as

$$\frac{\partial \Psi}{\partial t} + \nabla \cdot (\boldsymbol{u}\Psi) = \nabla \cdot \Omega + \sigma \tag{4}$$

where Ω is a tensor of one order greater than Ψ, σ a source term and $\boldsymbol{u}$ the velocity.

Taking the phase average of the quantity Ψ in the α-phase and applying the previous relations in Eq.(2) and Eq.(3) to the general transport equation, gives

$$\begin{aligned}\frac{\partial}{\partial t}\langle\Psi_\alpha\rangle + \nabla \cdot \langle \boldsymbol{u_\alpha}\Psi_\alpha\rangle + \frac{1}{V}\int_{A_{\alpha\beta}} \Psi(\boldsymbol{u_\alpha} - \boldsymbol{W_\alpha}) \cdot \boldsymbol{n_{\alpha\beta}}\,\mathrm{d}A \\ = \nabla \cdot \langle\Omega_\alpha\rangle + \int_{A_{\alpha\beta}} \Omega_\alpha \cdot \boldsymbol{n_{\alpha\beta}}\,\mathrm{d}A + \langle\sigma_\alpha\rangle\end{aligned} \tag{5}$$

Each field is decomposed into its phase average and a perturbation [17, 19, 15]

$$\begin{cases} \boldsymbol{u} = \langle \boldsymbol{u}\rangle + \tilde{\boldsymbol{u}} \\ \Psi = \langle\Psi\rangle + \tilde{\Psi} \end{cases} \tag{6}$$

This decomposition is applied to the previous development by considering the source term equal to zero and a static interface.

$$\begin{aligned}\frac{\partial}{\partial t}\langle\Psi_\alpha\rangle + \nabla \cdot (\langle \boldsymbol{u_\alpha}\rangle\langle\Psi_\alpha\rangle) + \nabla \cdot \langle\tilde{\Psi}_\alpha \tilde{\boldsymbol{u}}_\alpha\rangle \\ + \frac{1}{V}\int_{A_{\alpha\beta}} \Psi_\alpha \boldsymbol{u_\alpha} \cdot \boldsymbol{n_{\alpha\beta}}\,\mathrm{d}A \\ = \nabla \cdot \langle\Omega_\alpha\rangle + \frac{1}{V}\int_{A_{\alpha\beta}} \Omega_\alpha \cdot \boldsymbol{n_{\alpha\beta}}\,\mathrm{d}A\end{aligned} \tag{7}$$

2.2. Immersed microscopic heat transfer equations

In a porous medium at the grain or pore-scale, the conduction-convection heat transfers equations are described by the following system

$$\begin{cases} (\rho c_p)_s \dfrac{\partial T_s}{\partial t} = \nabla \cdot (k_s \nabla T_s) & \text{in } V_s \\ (\rho c_p)_f \frac{\partial T_f}{\partial t} + (\rho c_p)_f \nabla \cdot (\boldsymbol{u} T_f) = \nabla \cdot (k_f \nabla T_f) & \text{in } V_f \\ T_s = T_f & \text{at } A_{sf} \\ k_f \nabla T_f \cdot \boldsymbol{n_{sf}} = k_s \nabla T_s \cdot \boldsymbol{n_{sf}} & \text{at } A_{sf} \end{cases}$$

Following the method introduced by Peskin [20], this problem can be rewritten as a single equation defined over the entire domain of study. We consider the force $F(s,t)$ that represents the interfacial interactions. This force is taken into account as a source term

$$S = \int_A F(s,t)\delta(\boldsymbol{x} - \boldsymbol{X(s,t)})\,\mathrm{d}s \tag{8}$$

In the case of heat transfer, the mutual interaction between the fluid and the solid phases is expressed as the source term in the rewritten problem [21] as

$$\begin{aligned}\rho c_p \left(\frac{\partial T}{\partial t} + \nabla \cdot (\boldsymbol{u}T)\right) \\ = \nabla \cdot (k \nabla T) + \int_{A_{sf}} Q\delta(\boldsymbol{x} - \boldsymbol{X})\,\mathrm{d}S\end{aligned} \tag{9}$$

where

- $\rho c_p = \rho_f c_{p,f}$ in V_f
- $\rho c_p = \rho_s c_{p,s}$ in V_s
- $k = k_f$ in V_f
- $k = k_s$ in V_s
- $\boldsymbol{u} = \boldsymbol{u_f}$ in V_f
- $\boldsymbol{u} = \boldsymbol{0}$ in V_s

$\boldsymbol{x}$ and $\boldsymbol{X}$ represent the Eulerian and Lagrangian coordinates respectively and δ is a Dirac. The heat source Q is expressed with a jump function at the interface such that

$$Q = \left[k \frac{\partial T}{\partial n}\right] \tag{10}$$

where $[\,]$ is a jump function at the interface. Thanks to the condition of continuity of the heat flux at the interface, the immersed problem is therefore written as

$$\rho c_p \left(\frac{\partial T}{\partial t} + \nabla \cdot (\boldsymbol{u}T)\right) = \nabla \cdot (k \nabla T) \tag{11}$$

2.3. Homogenization

In the following development, we will consider a periodic medium. Let's begin by the first term of the generalized heat transfer equation considering that the interface velocity is zero.

$$\begin{aligned}\left\langle \frac{\partial T}{\partial t} \right\rangle &= \frac{\partial}{\partial t}\langle T\rangle - \frac{1}{V}\int_A T\boldsymbol{W} \cdot n\,\mathrm{d}A \\ &= \frac{\partial}{\partial t}\langle T\rangle\end{aligned}$$

Let us apply the the hypotheses of incompressibility and non-slip to the second term from of the left hand side. We obtain

$$\begin{aligned}\langle \nabla \cdot \boldsymbol{u}T \rangle &= \langle \nabla \cdot (T\boldsymbol{u}) - \cancel{T\nabla \cdot \boldsymbol{u}} \rangle \\ &= \nabla \cdot \langle T\boldsymbol{u} \rangle + \cancel{\frac{1}{V}\int_A T\boldsymbol{u} \cdot \boldsymbol{n}\, \mathrm{d}A}\end{aligned}$$

The perturbation decomposition Eq.(6) is introduced knowing that the average of the perturbation is zero.

$$\begin{aligned}\nabla \cdot \langle T\boldsymbol{u} \rangle &= \nabla \cdot [\langle \langle T \rangle \langle \boldsymbol{u} \rangle \rangle + \langle \langle T \rangle \tilde{\boldsymbol{u}} \rangle + \langle \tilde{T} \langle \boldsymbol{u} \rangle \rangle + \langle \tilde{T}\tilde{u} \rangle] \\ &= \nabla \cdot [\, \langle T \rangle \langle \boldsymbol{u} \rangle + \cancel{\langle T \rangle \langle \tilde{\boldsymbol{u}} \rangle} + \cancel{\langle \tilde{T} \rangle \langle \boldsymbol{u} \rangle} + \langle \tilde{T}\tilde{u} \rangle] \\ &= \langle \boldsymbol{u} \rangle \cdot \nabla \langle T \rangle + \nabla \cdot \langle \tilde{T}\tilde{u} \rangle\end{aligned}$$

Performing a magnitude analysis the last term is neglected. Then the right-hand term gives,

$$\begin{aligned}\langle \nabla \cdot (k \nabla T) \rangle = \nabla \cdot \left[k \left(\nabla \langle T \rangle + \frac{1}{V} \int_A \tilde{T} \boldsymbol{n}\, \mathrm{d}A \right) \right] \\ + \frac{1}{V} \int_A k \nabla \tilde{T} \cdot \boldsymbol{n}\, \mathrm{d}A\end{aligned}$$

Following the procedure described in [22], to obtain a closed form of the transport equation, it is necessary to substitute the result of the homogenization to the initial microscopic equations. Introducing the mapping vector $\boldsymbol{b}$ as [23, 24]

$$\tilde{T} = \boldsymbol{b} \cdot \nabla \langle T \rangle \tag{12}$$

the closure problem takes the form

$$(\rho c_p)\tilde{\boldsymbol{u}} + (\rho c_p)\boldsymbol{u} \cdot \nabla \boldsymbol{b} = k \nabla^2 \boldsymbol{b} \tag{13}$$

and the effective thermal conductivity is shown to write

$$\begin{aligned}\bar{\bar{k}} = [\epsilon k_f + (1-\epsilon)k_s]\, \bar{\bar{I}} + \frac{k_f - k_s}{V} \int_{A_{sf}} \boldsymbol{n_{sf}} \boldsymbol{b_f} \mathrm{d}A \\ - (\rho c_p)_f \langle \tilde{\boldsymbol{u}}\, \boldsymbol{b_f} \rangle^f\end{aligned} \tag{14}$$

The first term is the arithmetic average of the phase conductivities. The second term is a correction that captures the tortuosity of the fluid-solid interface. The last one is called the dispersion; it accounts for the local modifications of the heat flux by the internal flow [23, 10].

ϵ is the fluid volume fraction and $\boldsymbol{b_f}$ is determined from $\boldsymbol{b}$ with a phase indicator.

2.4. Numerical methods

The perturbation velocity is needed to determine $\boldsymbol{b_f}$ that is also needed to evaluate the dispersion term of the effective thermal conductivity. To obtain the perturbation velocity, an immersed boundary solver has been developed in OpenFoam using a SIMPLE pressure–velocity coupling procedure [25]. It solves the following system of equations

$$\begin{cases} \nabla \cdot \boldsymbol{u} &= 0 \\ \nabla \cdot (\boldsymbol{u} \otimes \boldsymbol{u}) &= -\nabla p + \nabla \cdot \tau - \mu K^{-1} \boldsymbol{u} \end{cases} \tag{15}$$

in the fluid and solid domain with a penalization term $\mu K^{-1}\boldsymbol{u}$ applied to the momentum conservation equation [26, 27]. The permeability K varies spatially to make the penalization term dominant in the solid zone and negligible in the fluid zone. The perturbation velocity is obtained from Eq.(6) and it is used to solve the closure problem Eq.(13). The field $\boldsymbol{b}$ is a solution of Eq.(13) up to a constant. To converge to the right solution, the problem is constrained by the average value of the mapping vector that should be zero. Finally, the closure problem is iteratively solved, a solution is obtained for the mapping vector and the dispersion is computed.

3. TEST CASE AND COMPARISON WITH THE LITERATURE

3.1. Description of the test case

The pore-scale geometry considered is a periodic array of circular cylinders of porosity $\epsilon = 0.37$. The ratio of solid and fluid thermal conductivities is 100. The flow is computed in a unit cell at a low Reynolds number. This problem was selected as a verification case as it has been studied by Quintard et al and DeGroot et al [14, 10].

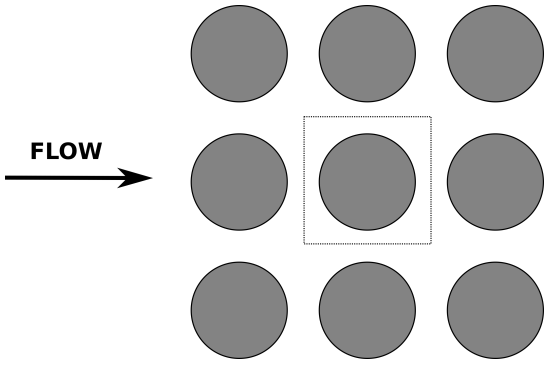

Fig. 2. Periodic array of cylinder considered with a unit cell in dashed line

3.2. Grid resolution study

According to DeGroot et al [22], at high Péclet number, a highly refined mesh is required to reach convergence. As shown in Fig. 3, the mesh used for our immersed problem is Cartesian. We carried out our own mesh convergence study.

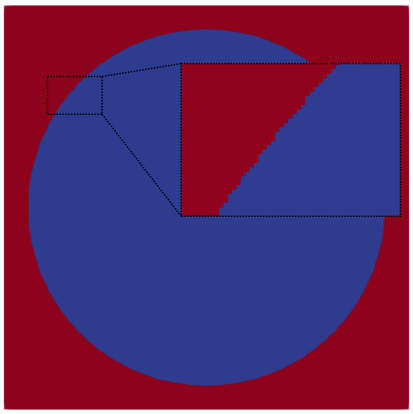

Fig. 3. Close-up view of solid-fluid interface

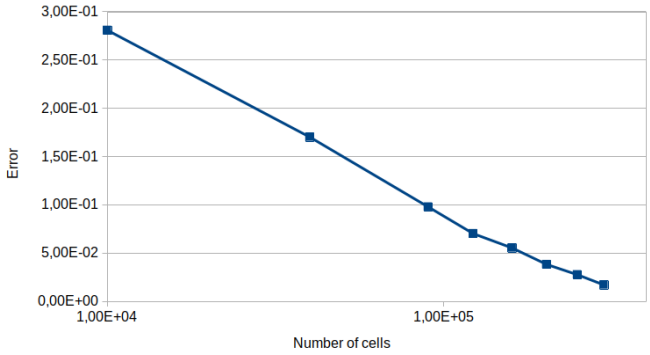

Fig. 4. Relative error for Pe = 500

To quantify the impact of mesh refinement on the results, the relative error between simulation and reference value is defined such that

$$error = \frac{k_{dn} - k_{dref}}{k_{dref}} \tag{16}$$

$$Pe = \frac{\rho_f \langle \boldsymbol{u} \rangle^f c_{p,f} d}{k_f} \tag{17}$$

The index n indicates the numerical simulation mesh refinement and k_d the dispersion term of the effective thermal conductivity in the x-direction. The reference value is given by [14]. The characteristic length used in the Péclet number is the unit cell length. The Péclet number selected to do the mesh convergence is 500. As shown in Fig. 4, the error decay is in agreement with the grid-size.

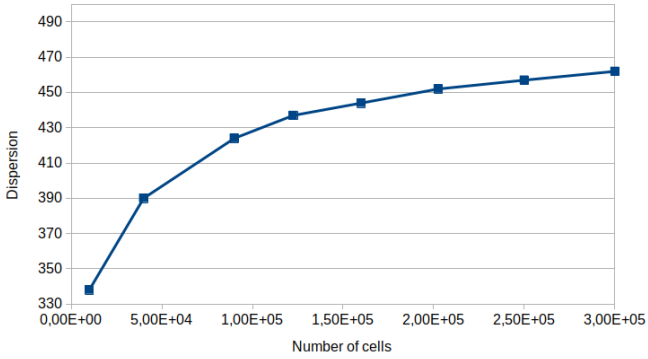

Fig. 5. Dispersion in function of the number of cells for Pe = 500

Fig. 5 shows the convergence trend. For the most refined mesh, the final error is 1%. Based on this analysis, the 300.000 cells-mesh is used in what follows.

3.3. Validation of the dispersion with literature

The test case of the array of cylinders is therefore used to compare the results obtained with the literature to validate our overall strategy. We compare the dispersion divided by the fluid thermal conductivity as a function of the Péclet number with DeGroot et al and Quintard et al for a low Reynolds number.

$$\bar{\bar{k}}_d = -\rho_f c_{p,f} \langle \tilde{\boldsymbol{u}} \boldsymbol{b} \rangle^f \tag{18}$$

$$\bar{\bar{k}}_{comp} = \bar{\bar{I}} + \frac{\bar{\bar{k}}_d}{k_f} \tag{19}$$

Figure Fig. 6 shows the velocity field in the domain obtained with the penalization method.

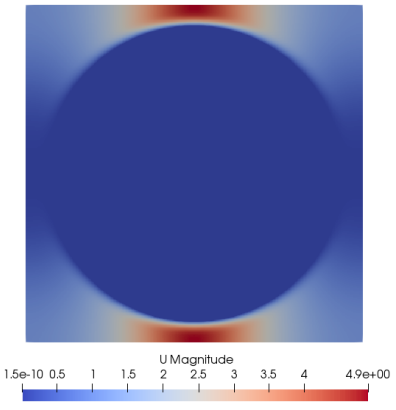

Fig. 6. Velocity field in the unit cell $\langle \boldsymbol{u} \rangle^f = (1; 0; 0)$

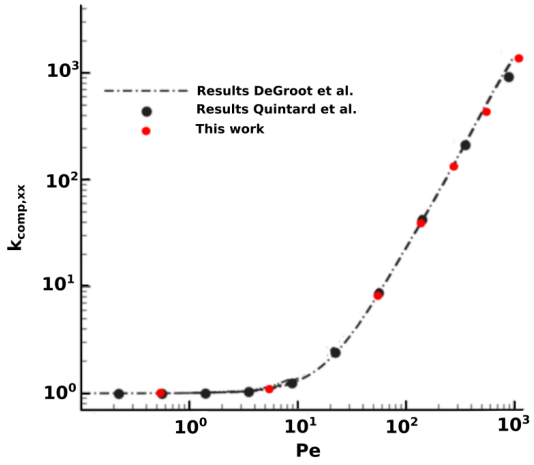

Fig. 7. Plot of the dimensionless dispersion part of the effective thermal conductivity in the axial direction for Re = 1

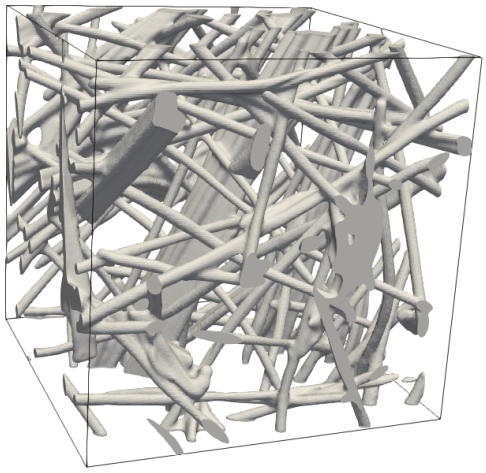

Fig. 8. Volume rendering of the tomography of Calcarb

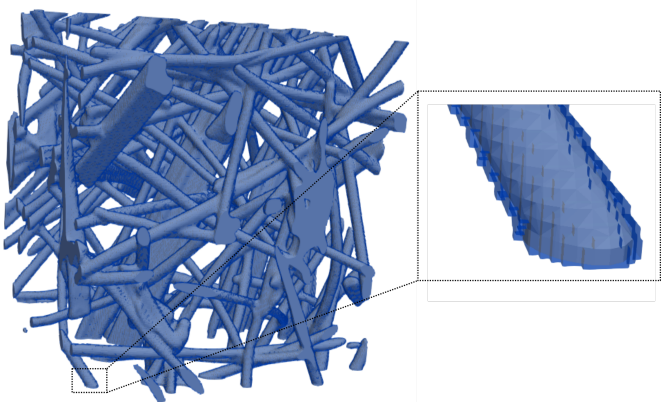

Fig. 9. Close-up view of the microstructure of Calcarb approximated by a Cartesian mesh.

The results presented in Fig. 7 show that the strategy developed in this work provides results in agreement with the literature. Indeed, on this test case the dispersion part of the effective thermal conductivity obtained in this work is in agreement with the results of DeGroot et al and Quintard et al on a wide range of Péclet number for a high thermal conductivity ratio. Results are also in good agreement for the others components of $\bar{\bar{k}}_{comp}$.

4. APPLICATION TO A TOMOGRAPHY OF CALCARB

The evaluation of the dispersion contribution to the effective thermal conductivity being validated on a reference problem, the same procedure will now be applied to a tomography of Calcarb.

Carbon fiber preforms, such as Calcarb are used as skeleton in heat-shield materials with a high average porosity. The digital representation of its micro-structure has been acquired at the Advanced Light Source (ALS) at Lawrence Berkeley National Laboratory and more details can be found in Borner et al, 2017 [28]. The domain is considered large enough to be representative. In order to make the domain periodic, we will add a thin layer of fluid mesh around the domain. This method, which is evaluated and discussed in [29], allows solving the closure problem on non-periodic domains with good accuracy. The geometry is always approximated using a Cartesian mesh and this creates mesh slots when the geometry is approached.

The porosity of the approximated geometry represented in Fig. 9 has been evaluated in order to select a relevant mesh refinement, knowing the real porosity of the material $\epsilon = 0.913$ [28].

The study of the convergence of the porosity Fig. 10 leads us to use the 42 million mesh. Indeed, this one seems to be a good compromise between a moderate number of cells for the simulation time and a good approximation of the true geometry. The fluid-solid thermal conductivity ratio is still used as being equal to 100. The characteristic distance used for the Péclet number is the average distance between two pores given by [29] and equal to $135\,\mu\mathrm{m}$.

The results obtained are presented in Fig. 11. They highlight the impact of the dispersion on the effective thermal conductivity. Dispersion is stronger in the flow direction than in the perpendicular directions.

The thermal conductivity of carbon fibers is about 2 W/m/K. The thermal conductivity of gases at room temperature is about 0.02 W/m/K. The effective conductivity of Calcarb is about 0.2 W/m/K. In this study, the dispersion term becomes important for a Péclet number above 1, that is, a gas flow velocity of 0.1 m/s.

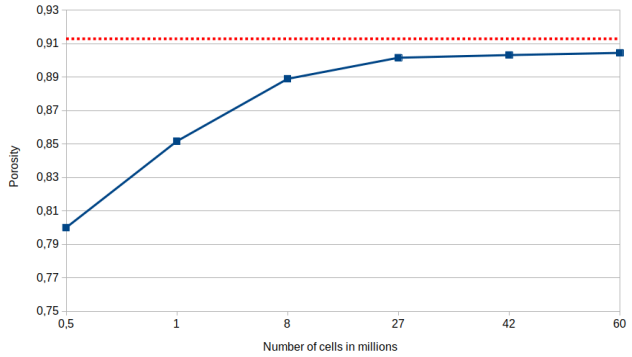

Fig. 10. Comparison between the real porosity of the geometry (dotted red line) and the porosity calculated with the approximate geometry (blue line).

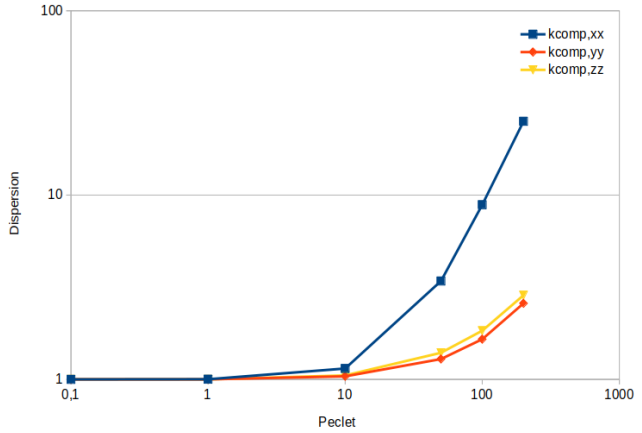

Fig. 11. Evolution of the dispersion Eq.(19) in function of the Péclet number for the Calcarb geometry

5. CONCLUSION

This study investigates the impact of dispersion on the effective thermal conductivity. To this end, the homogenisation of the microscopic heat transfer equation has been carried out with the volume averaging method. The closure problem has been implemented in PATO. The solver has been validated on a reference problem from the literature. The strategy has then been applied to a tomography of Calcarb. This study highlights the impact of convection on the effective conductivity of fibrous materials. The effect increases with the Péclet number that is related to the gas velocity. Dispersion is showed to increase significantly the thermal conductivity of Calcarb for gas velocities above 0.1 m/s. Further studies will be needed to evaluate the impact of this phenomenon, so far neglected, in flight conditions.

6. REFERENCES

[1] John David Anderson, *Hypersonic and high temperature gas dynamics*, AIAA, 2000.

[2] G. Duffa, *Ablative thermal protection systems modeling*, AIAA Educ. Ser., 2013.

[3] D. M. Curry, "Space shuttle orbiter thermal protection system design and flight experience," *NASA TM*, vol. 104773, pp. 1–22, 1993.

[4] H. K. Tran, C. E. Johnson, D. J. Rasky, F. C. L. Hui, M.-T. Hsu, T. Chen, Y. K. Chen, D. Paragas, and L. Kobayashi, "Phenolic impregnated carbon ablators (PICA) as thermal protection systems for discovery missions," *NASA Technical Memorandum*, vol. 110440, pp. 1–70, 1997.

[5] Kerry A. Trumble, Ioana Cozmuta, Steve Sepka, Peter Jenniskens, and Michael Winter, "Postflight aerothermal analysis of stardust sample return capsule," *Journal of Spacecraft and Rockets*, vol. 47, no. 5, pp. 765–774, 2010.

[6] Michael J Wright, Robin AS Beck, Karl T Edquist, David Driver, Steven A Sepka, Eric M Slimko, and William H Willcockson, "Sizing and margins assessment of mars science laboratory aeroshell thermal protection system," *Journal of Spacecraft and Rockets*, vol. 51, pp. 1025–1038, 2014.

[7] Todd R. White, Milad Mahzari, Ruth A. Miller, Chun Y. Tang, Chris D. Karlgaard, Hannah Alpert, Henry S. Wright, and Chris Kuhl, *Mars Entry Instrumentation Flight Data and Mars 2020 Entry Environments*.

[8] Mickael Rivier, Jean Lachaud, and Pietro Marco Congedo, "Ablative thermal protection system under uncertainties including pyrolysis gas composition," Research Report RR-9175, Inria Bordeaux Sud-Ouest, May 2018.

[9] Hannah Alpert, Milad Mahzari, David Saunders, Joshua Monk, and Todd R. White, *Inverse Estimation of Mars 2020 Entry Aeroheating Environments Using MEDLI2 Flight Data*.

[10] M. Quintard, M. Kaviany, and S. Whitaker, "Two-medium treatment of heat transfer in porous media: numerical results for effective properties," *Adv. Water Resour.*, vol. 20, no. 2-3, pp. 77–94, 1997.

[11] Jörg Petrasch, Birte Schrader, Peter Wyss, and Aldo Steinfeld, "Tomography-Based Determination of the Effective Thermal Conductivity of Fluid-Saturated Reticulate Porous Ceramics," *Journal of Heat Transfer*, vol. 130, no. 3, 2008.

[12] Francesco Panerai, Joseph C. Ferguson, Jean Lachaud, Alexandre Martin, Matthew J. Gasch, and Nagi N. Mansour, "Micro-tomography based analysis of thermal conductivity, diffusivity and oxidation behavior of rigid and flexible fibrous insulators," *International Journal of Heat and Mass Transfer*, vol. 108, pp. 801–811, 2017.

[13] Nima Nouri, Francesco Panerai, Kaveh A. Tagavi, Nagi N. Mansour, and Alexandre Martin, "Evaluation of the anisotropic radiative conductivity of a low-density carbon fiber material from realistic microscale imaging," *International Journal of Heat and Mass Transfer*, vol. 95, pp. 535–539, 2016.

[14] Christopher T. DeGroot and Anthony G. Straatman, "Closure of non-equilibrium volume-averaged energy equations in high-conductivity porous media," *International Journal of Heat and Mass Transfer*, vol. 54, no. 23, pp. 5039–5048, 2011.

[15] Yohan Davit, Christopher G. Bell, Helen M. Byrne, Lloyd A.C. Chapman, Laura S. Kimpton, Georgina E. Lang, Katherine H.L. Leonard, James M. Oliver, Natalie C. Pearson, Rebecca J. Shipley, Sarah L. Waters, Jonathan P. Whiteley, Brian D. Wood, and Michel Quintard, "Homogenization via formal multiscale asymptotics and volume averaging: How do the two techniques compare?," *Advances in Water Resources*, vol. 62, pp. 178–206, 2013, A tribute to Stephen Whitaker.

[16] Stephen. Whitaker, "Advances in theory of fluid motion in porous media," *Industrial & Engineering Chemistry*, vol. 61, no. 12, pp. 14–28, 1969.

[17] William G. Gray, "A derivation of the equations for multi-phase transport," *Chemical Engineering Science*, vol. 30, pp. 229–233, 1975.

[18] Serge BORIES, Abdelkader MOJTABI, Marc PRAT, and Michel QUINTARD, "Transferts de chaleur dans les milieux poreux: Conduction, convection, rayonnement," *Techniques de l'ingénieur. Génie énergétique*, 2008.

[19] Stephen Whitaker, "The transport equations for multiphase systems," *Chemical Engineering Science*, vol. 28, no. 1, pp. 139–147, 1973.

[20] Charles S Peskin, "Flow patterns around heart valves: A numerical method," *Journal of Computational Physics*, vol. 10, no. 2, pp. 252–271, 1972.

[21] Yang Hu, Decai Li, Shi Shu, and Xiaodong Niu, "Simulation of steady fluid–solid conjugate heat transfer problems via immersed boundary-lattice boltzmann method," *Computers Mathematics with Applications*, vol. 70, no. 9, pp. 2227–2237, 2015.

[22] Christopher DeGroot and Anthony Straatman, *Thermal Dispersion in High-Conductivity Porous Media*, pp. 153–180, 06 2012.

[23] Michel Quintard, "Introduction to heat and mass transport in porous media," *Porous Media Interaction with High Temperature and High Speed Flows, Von Karman Institude for Fluid Dynamics, Rhode Saint Genese, Belgium*, 2015.

[24] M. Kaviany, *Principles of Heat Transfer in Porous Media*, pp. 547–572, Mechanical Engineering Series. Springer New York, 1995.

[25] Suhas V Patankar, *Numerical heat transfer and fluid flow*, Series in Computational and Physical Processes in Mechanics and Thermal Sciences, 1980.

[26] C. Soulaine and H.A Tchelepi, "Micro-continuum approach for pore-scale simulation of subsurface processes," *Transp Porous Med*, vol. 113, pp. 431–456, 2016.

[27] K. Vafai and C.L Tien, "Boundary and inertia effect on flow and heat transfer in porous media," *International Journal of Heat and Mass Transfer*, vol. 24, pp. 195–203, 1981.

[28] Arnaud Borner, Francesco Panerai, and Nagi N. Mansour, "High temperature permeability of fibrous materials using direct simulation monte carlo," *International Journal of Heat and Mass Transfer*, vol. 106, pp. 1318–1326, 2017.

[29] H. Scandelli, A. Ahmadi-Senichault, C. Levet, and J. Lachaud, "Computation of the permeability tensor of non-periodic anisotropic porous media from 3d images," *Transp Porous Med*, 2022.